OXFORD GENETICS

GENETICS, 2021, 217(1), iyaa029
DOI: 10.1093/genetics/iyaa029
Advance Access Publication Date: 22 December 2020
Investigation

Proper CycE–Cdk2 activity in endocycling tissues requires regulation of the cyclin-dependent kinase inhibitor Dacapo by dE2F1b in Drosophila

Minhee Kim , Keemo Delos Santos, and Nam-Sung Moon *

Department of Biology, Developmental Biology Research Initiative, McGill University, Montreal, Quebec H3A 1B1 Canada

*Corresponding author: Department of Biology, Developmental Biology Research Initiative, McGill University, Montreal, Quebec, H3A 1B1 Canada. nam.moon@mcgill.ca

Abstract

Polyploidy is an integral part of development and is associated with cellular stress, aging, and pathological conditions. The endocycle, comprised of successive rounds of G and S phases without mitosis, is widely employed to produce polyploid cells in plants and animals. In Drosophila, maintenance of the endocycle is dependent on E2F-governed oscillations of Cyclin E (CycE)–Cdk2 activity, which is known to be largely regulated at the level of transcription. In this study, we report an additional level of E2F-dependent control of CycE–Cdk2 activity during the endocycle. Genetic experiments revealed that an alternative isoform of Drosophila *de2f1*, dE2F1b, regulates the expression of the $p27^{CIP/KIP}$-like Cdk inhibitor Dacapo (Dap). We provide evidence showing that dE2F1b-dependent Dap expression in endocycling tissues is necessary for setting proper CycE–Cdk2 activity. Furthermore, we demonstrate that dE2F1b is required for proliferating cell nuclear antigen expression that establishes a negative feedback loop in S phase. Overall, our study reveals previously unappreciated E2F-dependent regulatory networks that are critical for the periodic transition between G and S phases during the endocycle.

Keywords: Drosophila; endocycle; E2F; cyclin E; Dacapo; PCNA; S phase

Introduction

Across many organisms, a variant cell cycle called the endocycle, composed of G and S phases without cellular division, is commonly employed as a developmental growth strategy or as a wound-healing response (Orr-Weaver 2015). Endocycling cells undergo periodic doubling of the genome although specific genomic loci such as heterochromatic regions remain underreplicated (Lilly and Duronio 2005; Nordman *et al.* 2011; Sher *et al.* 2012; Yarosh and Spradling 2014). The endocycle harbors many similarities with the G1-S transition of the mitotic cycle, in which controlling the activity of cyclin-dependent kinases (Cdks) is crucial. Major differences between them occur at the end of S phase. While Cdk activity increases during the mitotic cycle, endocycling cells lower Cdk activity. Dampened Cdk activity is required for preventing mitosis and promoting pre-replicative complex (pre-RC) formation during the subsequent G phase of the endocycle (Edgar *et al.* 2014). As a consequence, silencing the mitotic Cdk activity and oscillation of the S-phase Cdk activity are crucial for the proper progression of the endocycle.

At the center of the endocycle are E2F transcription factors (Edgar *et al.* 2014). E2F targets include genes that are required for proper DNA synthesis, such as *Proliferating Cell Nuclear Antigen (PCNA) and Ribonucleoside Diphosphate Reductase Small Subunit (rnrS)*, as well as genes that are important for the G2/M transition (Dimova and Dyson 2005). E2Fs are classified based on their effect on transcription, as activator or repressor E2Fs. Cell cycle-dependent expression of E2F targets is achieved by the family of Retinoblastoma (Rb) proteins, which bind to and inhibit E2Fs. During the cell cycle, Rb proteins are phosphorylated and inactivated by Cdks (Rubin *et al.* 2020). In mice, the balance between activator E2Fs, E2F 1-3, and repressor E2Fs, E2F7, and 8, coordinates the endoreplication gene expression program (Chen *et al.* 2012; Pandit *et al.* 2012). For example, E2F7 and 8 repress genes involved in the G2/M transition and cytokinesis to favor the endocycle over mitosis. In Drosophila, endocycle-specific defects were observed in three independent alleles of the activator E2F, *de2f1* (Royzman *et al.* 1999, 2002; Weng *et al.* 2003; Kim *et al.* 2018). Moreover, dE2F1 activity is generally dampened in endocycling tissues compared to mitotic tissues (Maqbool *et al.* 2010). In general, E2F proteins are critical in establishing a proper transcriptional program in endocycling tissues.

Drosophila is an excellent system to investigate the mechanism of endocycle progression. Different degrees of polyploidy are achieved via the endocycle in various tissues such as the larval salivary gland, fat body, subperineurial glia, ovarian follicle, and nurse cells (NCs) (Orr-Weaver 2015). The salivary gland is widely used to study the mechanism of endocycle progression, where cells reach up to 1024C. In this tissue, the oscillatory relationship between dE2F1 and the S-phase Cyclin, Cyclin E (CycE) has been extensively studied (Edgar *et al.* 2014). dE2F1

Received: November 08, 2020. **Accepted:** December 6, 2020

accumulation during G phase promotes the timely expression of CycE and Cdk2 activity upon S-phase entry. High CycE-Cdk2 activity in S phase prevents origin relicensing by stabilizing Geminin via the inactivation of the anaphase-promoting complex/cyclosome (Narbonne-Reveau *et al.* 2008; Zielke *et al.* 2008). Germinin is a negative regulator of the licensing factor Double Parked (DUP)/Cdt1 (Whittaker *et al.* 2000). During S phase, degradation of dE2F1 is carried out by $CRL4^{Cdt2}$, an E3 ubiquitin ligase, which targets dE2F1 via the PCNA Interacting Peptide (PIP) degron in a DNA-dependent manner (Shibutani *et al.* 2008; Zielke *et al.* 2011). This ensures proper downregulation of CycE-Cdk2 at the end of S phase. Although the PIP degron-dependent mechanism seems to be unique to Drosophila, limiting E2F activity upon entry to S phase in endocycling tissues is essential in mice as well. A crucial target of E2F7/8 is a mammalian activator E2F, E2F1 (Li *et al.* 2008; Moon and Dyson 2008; Chen *et al.* 2012; Pandit *et al.* 2012) and failure to limit E2F activity in E2F7/8 mutant mice results in ectopic mitotic cyclin expression in endocycling tissues (Chen *et al.* 2012; Pandit *et al.* 2012). Notably, E2F7/8 are targets of the activator E2Fs, creating a negative feedback network between E2F proteins (Kent and Leone 2019).

Endocycle plays a central role in the NCs of the Drosophila ovary as well. NCs reach 512 C-1024C to support oocyte development through the synthesis and transport of maternal materials (Dej and Spradling 1999). A unique feature of the NCs is in their distinct pattern of chromatin dynamics (Dej and Spradling 1999). For the first four endocycles, chromosomes exist as bulbous polytenes, which progressively condense into a blob-like morphology at the end of cycle 4. During the fifth endocycle, a mitosis-like state dissociates the 64 C polytene chromosomes into 32 chromatid pairs. Thus, the chromosomes appear dispersed at stage 5 and onward (Figure 1C). This transition is associated with the changes in DNA replication patterns. Before endocycle 5, NC chromosomes fully replicate both early replicating (mostly euchromatic) and late replicating (heterochromatic) regions. Upon chromosome dispersal, late replicating regions are under-replicated at various degrees (Hammond and Laird 1985; Dej and Spradling 1999). This change in chromatin structure promotes ribosomal synthesis and is required for proper oocyte development (Keyes and Spradling 1997; Dej and Spradling 1999; Volpe *et al.* 2001). Interestingly, dE2F1 and dDP, which is the heterodimeric partner of dE2F1, were shown to be important for proper NC chromosome organization and oocyte polarity (Myster *et al.* 2000; Royzman *et al.* 2002). However, the mechanism by which dE2F1 regulates these processes during oogenesis is currently unclear.

Recently, our lab reported the functional importance of an alternatively spliced isoform of *de2f1*, named *de2f1b*, for cell-cycle regulation (Kim *et al.* 2018). dE2F1b differs from the canonical *de2f1*, *de2f1a*, by the addition of a microexon that disrupts an important physical interaction between the Marked Box domain of dE2F1 and the C-terminal domain of Rbf1, the Drosophila Rb homolog (Supplementary Figure S1A). Importantly, *de2f1b* is enriched in the salivary gland and *de2f1b* mutants display severe growth defects in polyploid tissues such as the larval salivary gland and the ovary. In this study, we show that unrestrained CycE–Cdk2 activity causes the defects in *de2f1b* polyploid tissues. We provide evidence that *dacapo* (*dap*), a Cdk inhibitor, is a critical factor downstream of dE2F1b that limits CycE–Cdk2 activity. In addition to *dap*, dE2F1b-dependent expression of PCNA is required for the biphasic expression of dE2F1 and CycE during the endocycle of the salivary gland. Overall, our study demonstrates that one of the major functions of dE2F1b is to fine-tune CycE–Cdk2 activity and to establish a proper negative feedback network during endocycle progression.

Materials and methods

Fly strains

All fly strains and crosses were maintained at 25°C on standard cornmeal medium in a 12-hour light and dark cycle. The full list of stocks and genotypes for each experiment are provided in Supplementary Tables S1 and S2.

Immunostaining and EdU labeling

For salivary gland immunostaining, 80–85-h after egg-laying (AEL) salivary glands were fixed in 4% formaldehyde in 1XPBS for 20 min at room temperature (note: for anti-dE2F1, tissues were fixed at 4°C for 30 min). Tissues were then washed three times with 0.3% PBSTriton-X and then three times with 0.1%PBSTriton-X. Tissues were incubated in a 1% BSA blocking solution with an appropriate primary antibody overnight at 4°C then washed three times in 0.1%PBSTriton-X. The secondary antibody incubation was carried out for 3 h at room temperature, then tissues were washed four times in 0.1%PBSTriton-X, and mounted for imaging.

For ovary immunostaining, adult female ovaries were staged and collected at 3- to 5-day posteclosion in 1XPBS. Ovaries were then fixed in 4% formaldehyde and 0.001% NP-40 in 1XPBS with three volumes of heptane for 20 min. Ovaries were rinsed three times in 0.1%PBSTween20. Ovaries were then subject to 1 h of permeabilization in 1%PBSTritonX-100 then incubated in 1%BSA in 0.1% PBSTween20 for 1 h. Primary antibody incubation was performed overnight at 4°C with an appropriate antibody concentration in 1% BSA in 0.1%PBSTween20. Ovaries were rinsed three times in 0.1% PBSTween20. Secondary antibody incubation was performed for 3 h with appropriate antibody concentration in 1%BSA in 0.1% PBSTween20. Ovaries were rinsed four times in 0.1PBSTween20 and mounted for imaging.

The primary antibodies used in this study are listed in Supplementary Table S3. The following secondary antibodies coupled to fluorescent dyes from Jackson ImmunoResearch were used in 1:200 dilutions: donkey anti-rabbit cy2, donkey anti-goat cy3, donkey anti-goat cy5, goat anti-mouse cy3, donkey anti-mouse cy5, and goat anti-guinea pig cy3. EdU cell proliferation assay (Invitrogen C10339) was used according to the manufacturer's specifications and dissected salivary glands and ovaries were incubated with EdU for 1 h in Schneider's medium (Sigma). DNA was visualized with 0.1 μg/ml DAPI. Representative images were selected from a minimum of 10 independent tissues.

Microscopy

All fluorescently labeled tissues were mounted using a glycerol-based anti-fade mounting medium containing 5% *N*-propyl gallate and 90% glycerol in 1XPBS. All salivary gland confocal micrographs were acquired using a laser-scanning Leica SP8 confocal microscope with a 20×/0.7 dry objective and all ovary confocal micrographs 63× oil-immersion objective as a Z-stack with 1.5 μm set as the Z-distance at the Cell Imaging and Analysis Network, McGill University. Representative images are from a minimum of 10 independent confocal micrographs were taken. Images from *in situ* hybridization experiments were taken using the Canon Powershot G10 and Zeiss SteREO Discovery V8 modular stereo microscope with a conversion lens adaptor. All images were processed using Fiji (http://fiji.sc/Fiji).

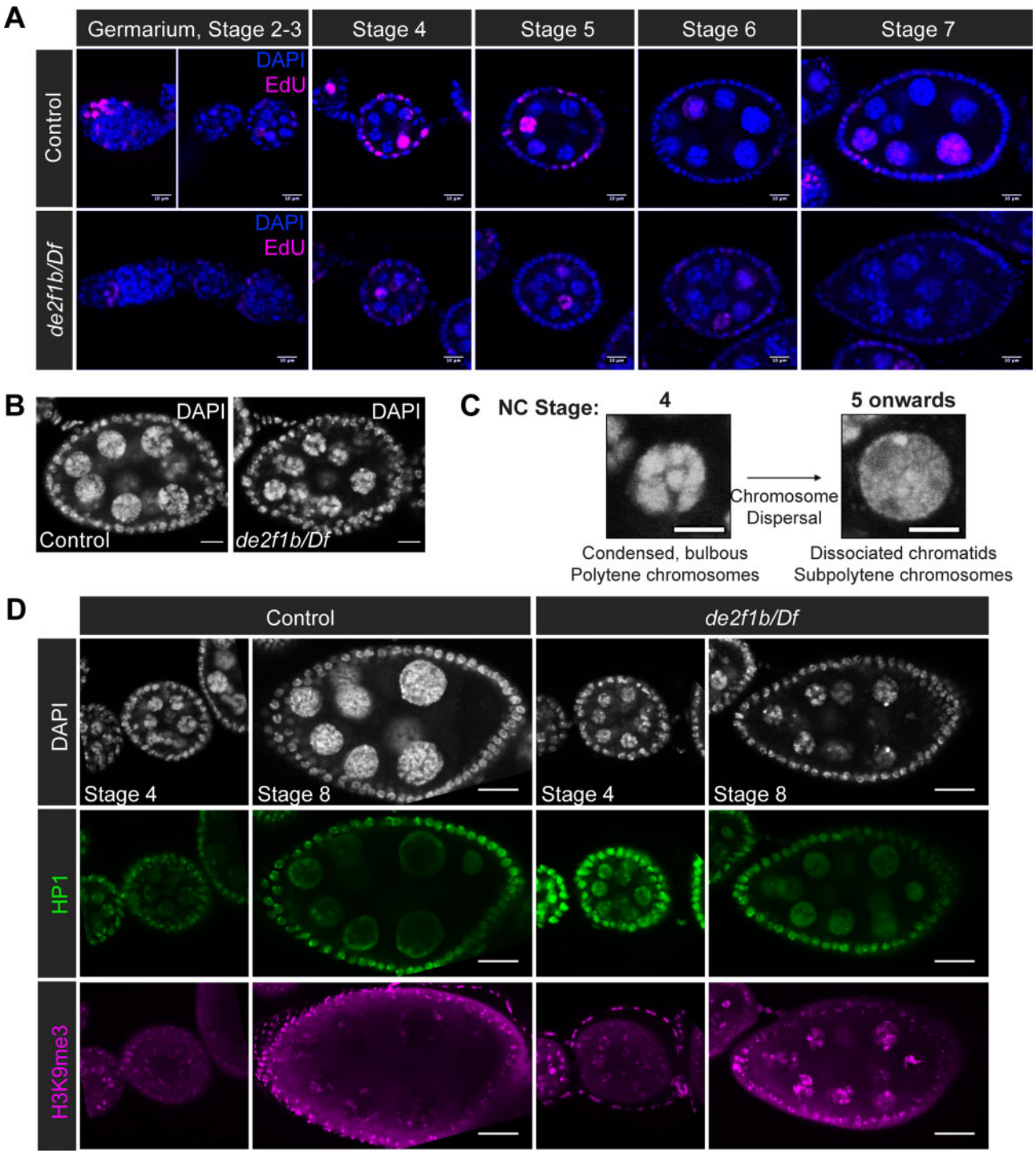

Figure 1 Impaired chromosomal dispersal in the NCs of *de2f1b* egg chambers. (A) Micrographs of egg chambers staged from germarium to stage 7 of oogenesis in control and *de2f1b/Df* ovaries marked with DAPI or EdU. Scale bar represents 10 μm. (B) Stage 6 egg chambers of control and *de2f1b*, where the aberrant shape of NCs was observed. Scale bar represents 10 μm. (C) A schematic representation of the chromosome dispersal process normally observed in the NC during stage 4 to stage 5 transition of oogenesis. Scale bar represents 5 μm. (D) DAPI, HP1, H3K9me3 staining of control and *de2f1b* egg chambers, showing bulbous chromosomes (stage 4) and dispersed chromosomes (stage 8). Scale bar represents 20 μm.

Generation of plot profile plots

Per genotype, a minimum of 250 μ was spanned across a section of the salivary gland through the middle of each nuclei using the freehand line tool in Fiji. The Plot Profile analysis tool was used to generate plots per individual channel. Generated plot profiles for two channels were merged on GraphPad Prism. The linearized image was created using the Straighten edit tool from Fiji.

Quantification of nuclear protein and DAPI intensities

Nuclear protein intensities for dE2F1, CycE, G1-FUCCI, EdU, DUP, Dap-Myc, PCNA, and DAPI were obtained through the mean fluorescent intensity values using the particle analysis tool in Fiji. For each salivary gland, a maximum Z-projection of two stacks from the most apical and most basal sections were produced then

subjected to analysis to accurately quantify the overall distribution of nuclear concentrations in a given salivary gland. Five independent salivary glands from the same experiment were analyzed to control for differential protein intensities. A minimum of 300 nuclei is shown for all analyses. Nuclear protein intensities were then plotted as an X, Y point plot or a scatter plot to show protein levels using GraphPad Prism or the ggplot2 package using R. Ploidy was plotted in a box and whiskers plot in GraphPad Prism.

Quantification of S-phase population

EdU incorporation positive nuclei were identified by the particle analysis tool in Fiji. For each salivary gland, the percentage of EdU incorporation positive nuclei per salivary gland was counted for five independent salivary glands from maximum Z-projection of two stacks from the most apical and most basal sections. The average of the S-phase populations taken from five salivary glands is shown. Error bars indicate standard deviation (SD).

Quantification of dE2F1:CycE ratio

Fluorescence intensities of dE2F1 and CycE were determined using the particle analysis tool in Fiji. For each nucleus, dE2F1 intensity was divided by CycE intensity then log-transformed (log base 10) to get values ranging from 1 to −1, where 0 represents the 1:1 ratio (labeled as a dotted line), values toward (max: 0.6) represent cells with higher dE2F1, and values toward −1 (min: −0.7) represent cells with higher CycE.

Quantification of the relative standard deviation of the nuclear area

The nuclear area was determined by using the particle analysis tool in Fiji. The relative standard deviation was calculated by dividing the standard deviation of nuclear size by the mean of the nuclear size per salivary gland. Three independent salivary glands were analyzed for each genotype. Error bars indicate SD.

Eclosion rate quantification

To quantify the eclosion rate, eggs were collected from each genotype for 1 day then total pupae that eclosed after 14 days AEL were counted and their eclosion rate was calculated accordingly in comparison to total pupae present. Values represent an average of experimental triplicates. Error bars indicate the SD.

RNA extraction and cDNA synthesis

For the ovary, RNA was extracted from 1-day old ovaries from Control and 2-day-old ovaries from *de2f1b* using the Aurum Total RNA Mini Kit (Bio-Rad) with the treatment of DNase I to remove genomic DNA contamination. In total, 500 ng of RNA was used to synthesize cDNA using the iScript cDNA Synthesis Kit (Bio-Rad).

For the salivary gland, RNA was extracted from 40 w^{1118} or *de2f1b* 80-85 h AEL salivary glands using the Aurum Total RNA Mini Kit (Bio-Rad) with the treatment of DNase I to remove genomic DNA contamination. In brief, 200 ng of RNA was used to synthesize cDNA using the iScript cDNA Synthesis Kit (Bio-Rad).

Quantitative reverse transcription PCR

Gene expression was quantified using the DyNAmo Flash SYBR Green qPCR Kit (Thermo-Scientific) with the comparative cycle method using the Bio-Rad CFX 96 Real-Time System and C1000 Thermal Cycler. Two housekeeping genes, *rp49* and β-*tubulin*, were used to normalize the data obtained. All values represent the averages of experimental biological triplicates and error bars represent SD. All primers were designed using Primer3 (Whitehead Institute for Biomedical Research, http://Frodo.wi.mit.edu/primer3/) or taken from the DRSC/TRiP Functional Genomics Resources FlyPrimerBank (Hu *et al.* 2013). All primers were tested and run on an 8% acrylamide gel to ensure a single PCR product. Primers used in this article are listed in Supplementary Table S4.

Statistical analysis

Statistical analyses were performed using the GraphPad Prism software. Two-tailed unpaired *t*-tests were performed and shown in Figures 2A, 4C, 4D, 6D, 6E, and 7B, and Supplementary Figure S2A. *F*-test was performed to calculate the variance and shown in Figures 4D and 6E. One-way ANOVA was performed and shown in Figures 7, D and E, Supplementary S2D, S3, A, E, and F. *P*-values represent ns = $P > 0.05$; *$P \leq 0.05$; **$P \leq 0.01$; ***$P \leq 0.001$; ****$P \leq 0.0001$.

In situ hybridization

Three- to five- day-old ovaries and 80–85 h AEL salivary glands were prepared for *in situ* hybridization as described previously (Du 2000). Briefly, samples were hybridization of DIG-labeled probes and then incubated with alkaline phosphatase-conjugated anti-DIG antibody (Roche) and detected using the NBT/BCIP stock solution (Roche). A minimum of 10 independent ovarioles was examined and representative images were selected. *rmrS*, *cycE* probes were generated as described previously (Hsieh *et al.* 2010) and the *dap* probe was prepared during this study (details are given in the Supplemental Methods section).

Data availability

The authors state that all data necessary for confirming the conclusions presented in the article are represented completely within the article. Supplementary information include supplemental methods, references, three supporting data figures (Supplementary Figures S1–S3), and tables containing the following lists: Drosophila stocks used in the study (Supplementary Table S1), full genotype of each experiment (Supplementary Table S2), primary antibodies (Supplementary Table S3), primer sequences (Supplementary Table S4), and genes involved in NC chromosome dispersal defect (Supplementary Table S5).

Supplemental material is available at fighsare DOI: https://doi.org/10.25386/genetics.13323023.

Results

de2f1b egg chambers have NCs with impaired chromosome dispersal at endocycle 5

To gain insights into the female sterility and size defect, which we reported in a previous study (Kim *et al.* 2018), the nuclear morphology of the developing egg chambers was visualized using 4,6-Diamidine-2′-phenylindole dihydrochloride (DAPI). Similar to the hypomorphic *de2f1* allele, $de2f1^{i2}$, *de2f1b* egg chambers contained abnormal NC nuclei with DAPI-intense foci (Royzman *et al.* 2002) (Supplementary Figure S1B). To understand the contribution of defects in cell-cycle progression, ethynyl deoxyuridine (EdU) incorporation was performed to visualize S-phase cells (Figure 1A). Unlike in the control where EdU incorporation was readily detected from germarium to stage 7 egg chamber, EdU incorporation was weaker and almost undetectable in stage 7 *de2f1b* egg chambers. In addition, the morphology of NC chromosomes in stages 6 and 7 of *de2f1b* egg chambers often remained bulbous (Figure 1, A and B). We also observed that *de2f1b* NCs have an

abnormal pattern of heterochromatic markers. In control egg chambers, HP1 and H3K9me3 signals were localized to the outer ring of the NC nuclei from stage 5 onward (Figure 1D, left panel). However, in *de2f1b* NCs, they were detected throughout the nucleus (Figure 1D, right panel). Taken together, these observations suggest that dE2F1b is required for the transition from condensed to dispersed chromosomes during the NC endocycles and for proper heterochromatin organization.

dE2F1b regulates the expression of G1/S phase genes, but not *cycE*

To better understand the NC defects, we determined how the expressions of canonical E2F targets are affected in *de2f1b* ovaries. Quantitative reverse transcription PCR (RT-qPCR) was performed on E2F targets that are important for G1/S or G2/M phases (Figure 2A). Interestingly, although G2/M E2F target genes were relatively unchanged, G1/S E2F target genes, such as *PCNA and rnrS*, were significantly reduced. Curiously, the expression of *cycE* did not follow the tendency of other G1/S E2F targets and remained relatively unchanged. These results were further validated by examination of promoter–reporter constructs and *in situ* hybridization. Although the expressions of *PCNA* and *rnrS* were reduced throughout oogenesis, the expression of *cycE* remained consistent in *de2f1b* ovaries (Figure 2, B–D). Notably, we observed a decrease in the transcript level of *dacapo* (*dap*) (Figure 2A), a $p27^{CIP/KIP}$-like Cdk inhibitor, which can inhibit CycE-Cdk2 activity (de Nooij *et al.* 1996). This was surprising since the targets of dE2F1 are normally associated with promoting cell-cycle progression and not with cell-cycle inhibition. However, the changes in the expression of gene suggested that dE2F1b regulates a specific subset of E2F targets in the ovary that are important for G1/S-phase transition.

Given that the expression of *dap* was reduced (Figure 2A), we hypothesized that CycE–Cdk2 activity may be deregulated in *de2f1b* ovaries. Supporting this notion, previous studies have demonstrated that deregulated CycE–Cdk2 activity results in the same chromosome dispersal defect as shown in Figure 1. *dap* mutants and a hypomorphic *cycE* allele that fail to properly downregulate CycE during S phase result in the same NC defect (Lilly and Spradling 1996; Hong *et al.* 2007). To monitor CycE–Cdk2 activity, we determined the expression pattern of DUP. DUP accumulates in G phase and is rapidly degraded at the onset of S phase (Thomer *et al.* 2004; Arias and Walter 2006; Jin *et al.* 2006; Senga *et al.* 2006). Importantly, previous studies have demonstrated that CycE–Cdk2 promotes DUP destruction (Thomer *et al.* 2004) and that the expression level of DUP is strongly reduced in *dap* mutant egg chambers (Hong *et al.* 2007). In *de2f1b* ovaries, NCs with nuclear DUP were absent while they were readily detected in the control (Figure 2E). Taken together, our result suggests that dE2F1b regulates a subset of G1/S phase genes, including *dap*, and that CycE–Cdk2 activity is likely increased in *de2f1b* egg chambers.

CycE–Cdk2 prevents NC chromosome dispersal in *de2f1b* ovary

To test if increased CycE–Cdk2 activity is responsible for the defects observed in *de2f1b* NCs, we partially depleted *cycE* via *heat-shock-Gal4* (*hs-Gal4*). Importantly, a partial *cycE* knockdown was achieved by maintaining the crosses at 25°C without providing any heat shock. This approach relies on the basal *hsp70* promoter activity (McGuire *et al.* 2004) and we have previously used this approach for partial *cycE* knockdown in the salivary gland (Kim *et al.* 2018). Upon knockdown of *cycE*, the chromosome dispersal defect was suppressed in *de2f1b* NCs (Figure 3A, yellow arrowheads). In addition, the abnormal pattern of HP1 staining in *de2f1b* NCs was no longer observed, resembling the pattern of control NCs (Figure 3B). We next determined if expressing Dap in *de2f1b* ovaries (Figure 2A) can also suppress the dispersal defect. Similar to *cycE* depletion, ectopic expression of Dap via *hs-Gal4* strongly suppressed the dispersal defect observed in *de2f1b* NCs (Figure 3C). In addition, nuclear expression of DUP was restored by Dap expression (Figure 3C). Overall, these results suggest that dE2F1b is required for limiting CycE–Cdk2 activity, which is critical for the proper transition from condensed to dispersed chromosome during NC endocycles.

dE2F1b is required for CycE and dE2F1 oscillations in endocycling salivary glands

To better understand the impact of the *de2f1b* mutation on the endocycle, we analyzed the larval salivary gland, which allows for a more precise and in-depth analysis of the endocycle. Importantly, we found similar dE2F1b-dependent transcriptional changes in the early third instar (L3) salivary glands (80–85 h AEL) to what was observed in the ovary (Supplementary Figure S2, A and B). It is important to note that the dE2F1b-dependent transcriptional changes that were previously reported are from late L3 salivary glands (105–110-h AEL) (Kim *et al.* 2018), whereas this study primarily uses early L3 salivary glands. In the previous study, we reported that the mutually exclusive expression pattern of dE2F1 and CycE is disrupted in the *de2f1b* mutant. To better illustrate this phenotype, 2D scatter plots of the dE2F1 and CycE were generated, where the relationship between dE2F1 and CycE in each cell is visualized (Figure 4A, right panels). In control salivary glands, the biphasic expression of dE2F1 and CycE is well-illustrated by their mutual exclusivity and clear separation of cell populations that exhibits high dE2F1 or high CycE levels (Figure 4A, control panel). This mutual exclusivity between dE2F1 and CycE was lost in *de2f1b* salivary glands, showing a linearized relationship between the two proteins (Figure 4A, *de2f1b* panel). Surprisingly, despite the overlapping expression of dE2F1 and CycE, S-phase cells were readily detected in *de2f1b* salivary glands, evidenced by the abundance of EdU-positive cells (Figure 4B). Notably, the percentage of S-phase cells in *de2f1b* salivary glands was significantly higher than in the control salivary glands (Figure 4C). Furthermore, although the mean CycE levels were not significantly different, cells with high CycE levels were lacking in *de2f1b* salivary glands, resulting in a significant decrease in the variance of CycE levels (Figure 4D). Although CycE high cells were scarce, the relationship between the expression of CycE and EdU incorporation remained relatively unchanged in *de2f1b* salivary glands (Figure 4E). Taken together, these data indicate that although dE2F1b is required for the oscillation of dE2F1 and expression of CycE, *de2f1b* mutant cells readily enter S phase during salivary gland endocycles.

Cyclin E-high G-phase cells are lacking in *de2f1b* salivary glands

To better determine the expression pattern of CycE relative to the G phase, the Fly-Fluorescent Ubiquitination-based Cell-Cycle Indicator (FUCCI) system was used (Zielke *et al.* 2014). In particular, the G1 sensor, hereon referred to as G1-FUCCI, was used to positively mark G-phase cells. G1-FUCCI is GFP fused to PIP box-dependent E2F1 degron ($GFP\text{-}E2F1_{1–230}$), which is targeted for degradation in an S phase-specific manner (Figure 5A) (Shibutani *et al.* 2008; Zielke *et al.* 2014). G- and S-phase cells were unambiguously identified via G1-FUCCI and EdU signals respectively (Figure 5B), in control salivary glands (Figure 5, C and D, left panels).

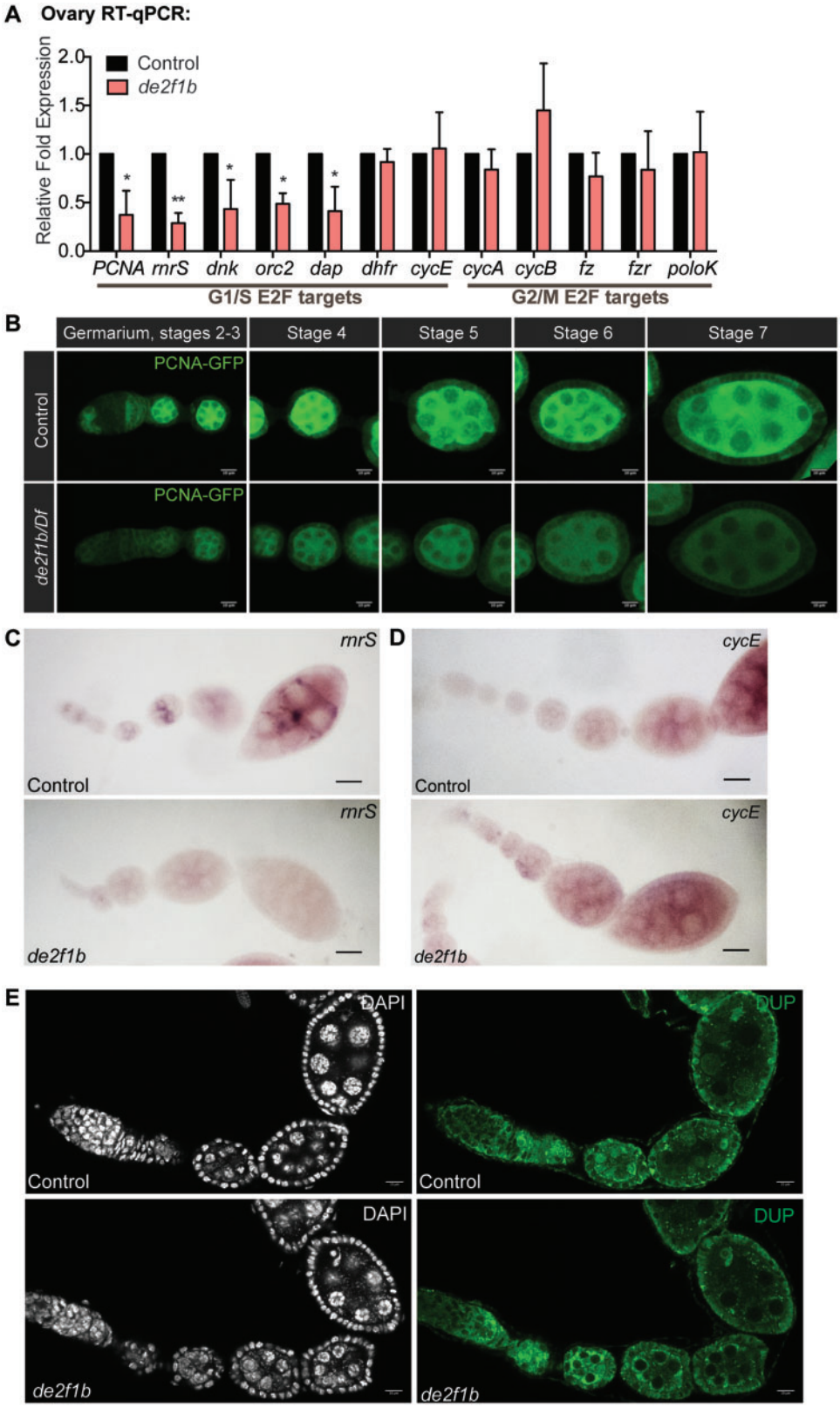

Figure 2 A subset of E2F target gene expression is affected in the *de2f1b* ovary. (A) RT-qPCR using 1-day old control and 2-day old *de2f1b* ovaries to compare young egg chambers. Two-day old *de2f1b* ovaries were used for collection to match the developmental stage and overall size of the control ovary. Error bars indicate the standard deviation (SD) from triplicated experiments. *$P \leq 0.05$; **$P \leq 0.01$. (B) Micrographs of PCNA-GFP expression in control (top panel) and *de2f1b* (bottom panel) ovaries. Scale bar represents 10 μm. (C, D) Micrographs of ovaries of control and *de2f1b* mutants showing (C) *rnrS* and (D) *cycE in situ* hybridization. Scale bar represents 25 μm. (E) Micrographs of control (top panel) and *de2f1b* (bottom panel) ovaries showing Dup expression (green) with DAPI staining (white). Scale bar represents 10 μm.

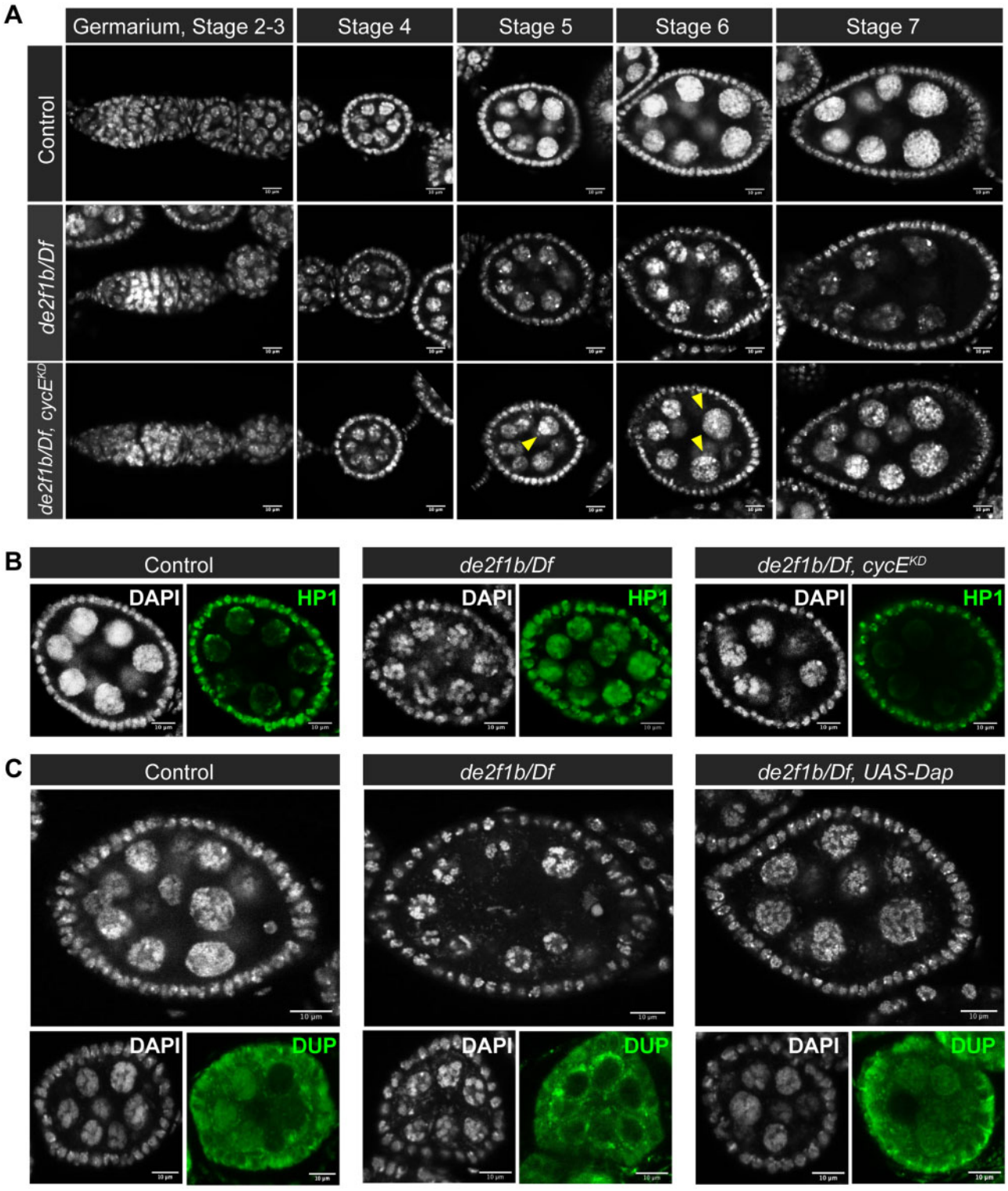

Figure 3 *cycE* knockdown allows chromosome dispersal in stage 5 *de2f1b* NCs. (A) Micrographs of control, *de2f1b*, and *de2f1b* with *cycE* depletion ($cycE^{KD}$) egg chambers. DAPI staining of egg chambers from germarium to stage 7 is shown. Yellow arrowhead indicates NC chromosome dispersal in *de2f1b* mutants upon $cycE^{KD}$. Scale bar represents 10 μm. (B) Micrographs of stage 6 egg chambers marked with DAPI (white) and HP1 (green) in control, *de2f1b/Df*, and *de2f1b/Df*, $cycE^{KD}$ backgrounds. Scale bar represents 10 μm. (C) Micrographs of stage 6 egg chambers stained with DAPI (upper panel) and stage 4 egg chambers marked with DAPI and DUP. Control, *de2f1b*, and *de2f1b* expressing Dap are shown. Scale bar represents 10 μm.

Interestingly, in *de2f1b* salivary glands, the separation between G1-FUCCI and EdU populations was less pronounced (Figure 5, C and D, right panels). This suggests that the S-phase-specific PIP box-dependent degradation mechanism is deregulated in *de2f1b* salivary glands, which likely contributes to the lack of mutual exclusivity between dE2F1 and CycE (Figure 4A).

Next, we compared the expression pattern of CycE relative to G1-FUCCI between control and *de2f1b* salivary glands

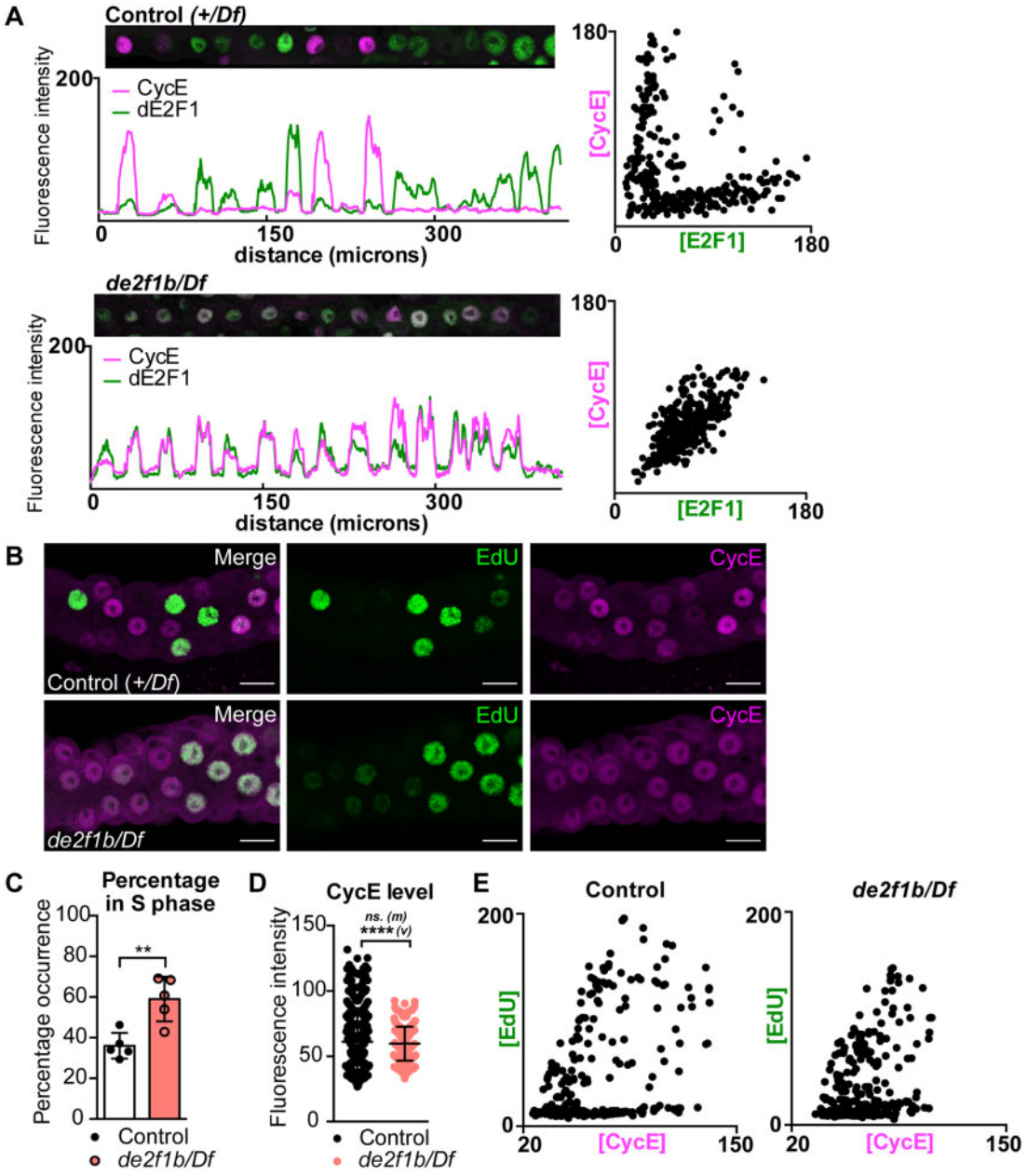

Figure 4 dE2F1b is required for CycE and dE2F1 oscillations and activates a subset of G1/S E2F targets in endocycling salivary glands. (A) A plot profile (left) and 2D scatter plot (right) depicting the nuclear intensities of dE2F1 (green) and CycE (magenta) from 80 to 85 h after AEL salivary gland cells in Control and *de2f1b/Df* salivary glands ($n = 5$/genotype). (B) Confocal micrographs of 80–85 h AEL Control and *de2f1b* salivary glands marked with EdU (green) and CycE (magenta). Scale bars = 25 μm. (C) Quantification of the percentage of EdU-positive cells ($n = 5$/genotype). Error bars indicate SD. $^{**}P \leq 0.01$. (D) A scatter plot depicting CycE protein intensity where the mean (m) CycE was not significantly different but the variance (v) was significantly changed between the two genotypes. ns = $P > 0.05$; $^{****}P \leq 0.0001$. (E) 2D scatter plots showing intensities of CycE and EdU between control and *de2f1b/Df* salivary gland cells ($n = 5$/genotype).

(Figure 5E). In control salivary glands, cells expressing high CycE are present in both G1-FUCCI low (S phase) and G1-FUCCI high (G phase) cells (Figure 5E, left panel). This demonstrates that high levels of CycE accumulate during G phase and that CycE levels may not directly reflect CycE–Cdk2 activity. We hypothesized that high CycE G-phase cells represent late G-phase cells that are primed to enter S phase. Importantly, although CycE high cells were scarce in *de2f1b* salivary glands, they were generally associated with low levels of G1-FUCCI and lacking from the high G1-FUCCI population (Figure 5E, right panel). Given that EdU-incorporating cells are readily detected in *de2f1b* salivary glands (Figure 4C), this suggests that the *de2f1b* cells do not require high levels of CycE to enter S phase.

Similar to the ovary, CycE–Cdk2 may be hyperactive in *de2f1b* salivary glands. The expression of DUP was strongly reduced in *de2f1b* salivary glands (Figure 5F) as seen in the ovary (Figure 3C). To test whether CycE–Cdk2 activity is altered in *de2f1b* salivary glands, anti-MPM-2 antibody staining was performed to label histone locus bodies in cells that have active CycE–Cdk2 (Calvi *et al.* 1998; White *et al.* 2007). A larger fraction of cells contained MPM-2 foci in *de2f1b* salivary glands (90.2% ± 6.4) than in control salivary glands (62.2% ± 3.2) (Supplementary Figure S2E). Furthermore, partial depletion of *cycE* in *de2f1b* salivary glands

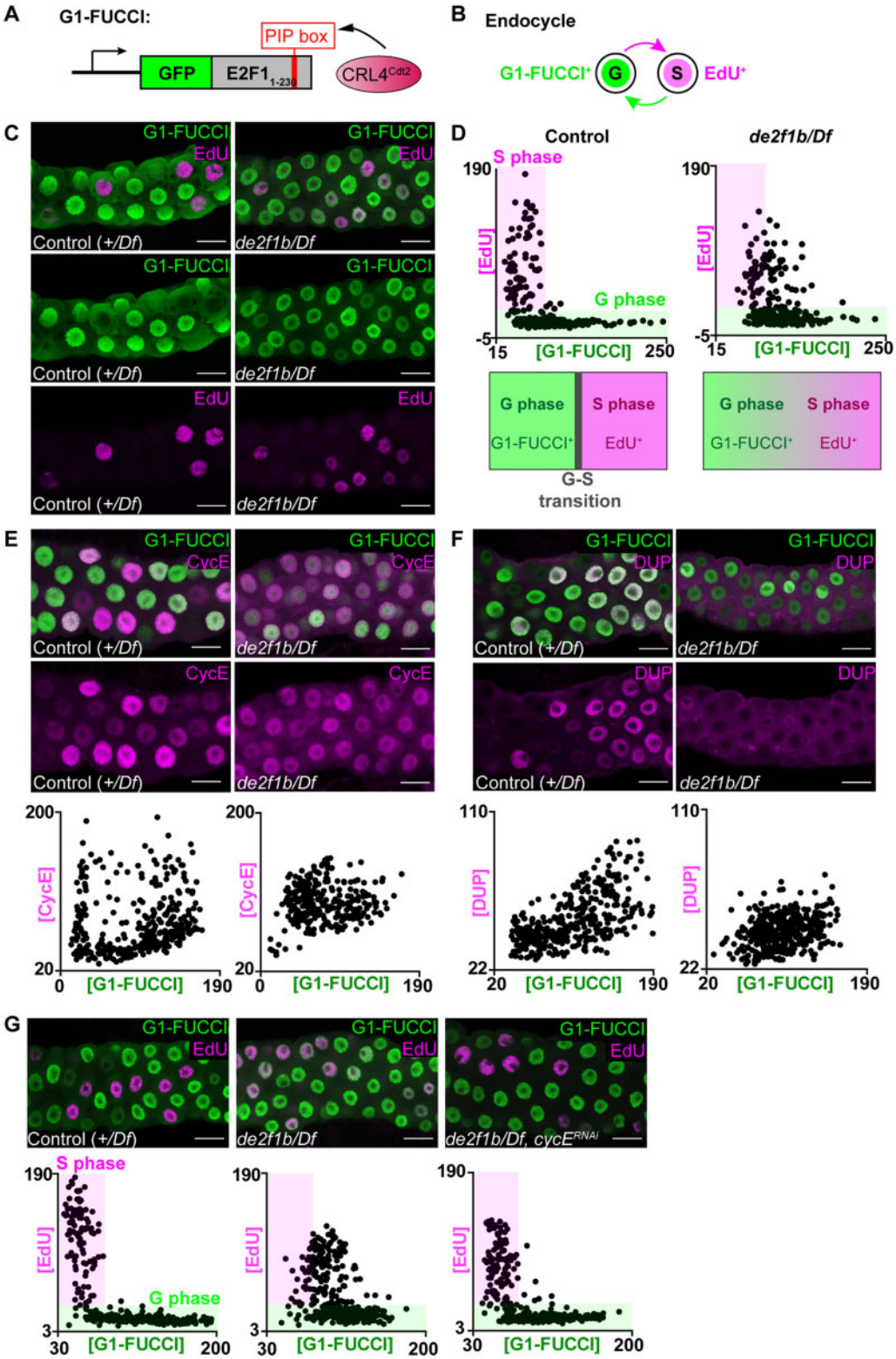

Figure 5 dE2F1b is required for CycE and dE2F1 oscillations in endocycling salivary glands (A) A schematic representation of G1-FUCCI, which contains the PIP box of E2F1 targeted by $CRL4^{Cdt2}$. (B) A schematic representation of describing the use of G1-FUCCI and EdU to visualize G- and S-phase cells, respectively. (C) Confocal micrographs of 80–85 h AEL salivary glands of control and *de2f1b/Df*. G- and S-phase cells are visualized via G1-FUCCI and EdU, respectively. (D) 2D scatter plots showing G1-FUCCI (green) and EdU (magenta) intensities of control and *de2f1b* salivary glands ($n = 5$/genotype). (E) Confocal micrographs (top panel) and 2D scatter plots (lower panel) of 80–85 h AEL control and *de2f1b/Df* salivary glands labeled with G1-FUCCI (green) and CycE (magenta) ($n = 5$/genotype). (F) Confocal micrographs (top panel) and 2D scatter plots (lower panel) of 80–85 h AEL control and *de2f1b/Df* salivary glands labeled with G1-FUCCI (green) and DUP (magenta) ($n = 5$/genotype). (G) Confocal micrographs (top panel) and 2D scatter plots (lower panel) of 80–85 h AEL control, *de2f1b*, and *de2f1b* with *cycE* depletion salivary glands labeled with G1-FUCCI (green) and EdU (magenta). All scale bars = 25 μm.

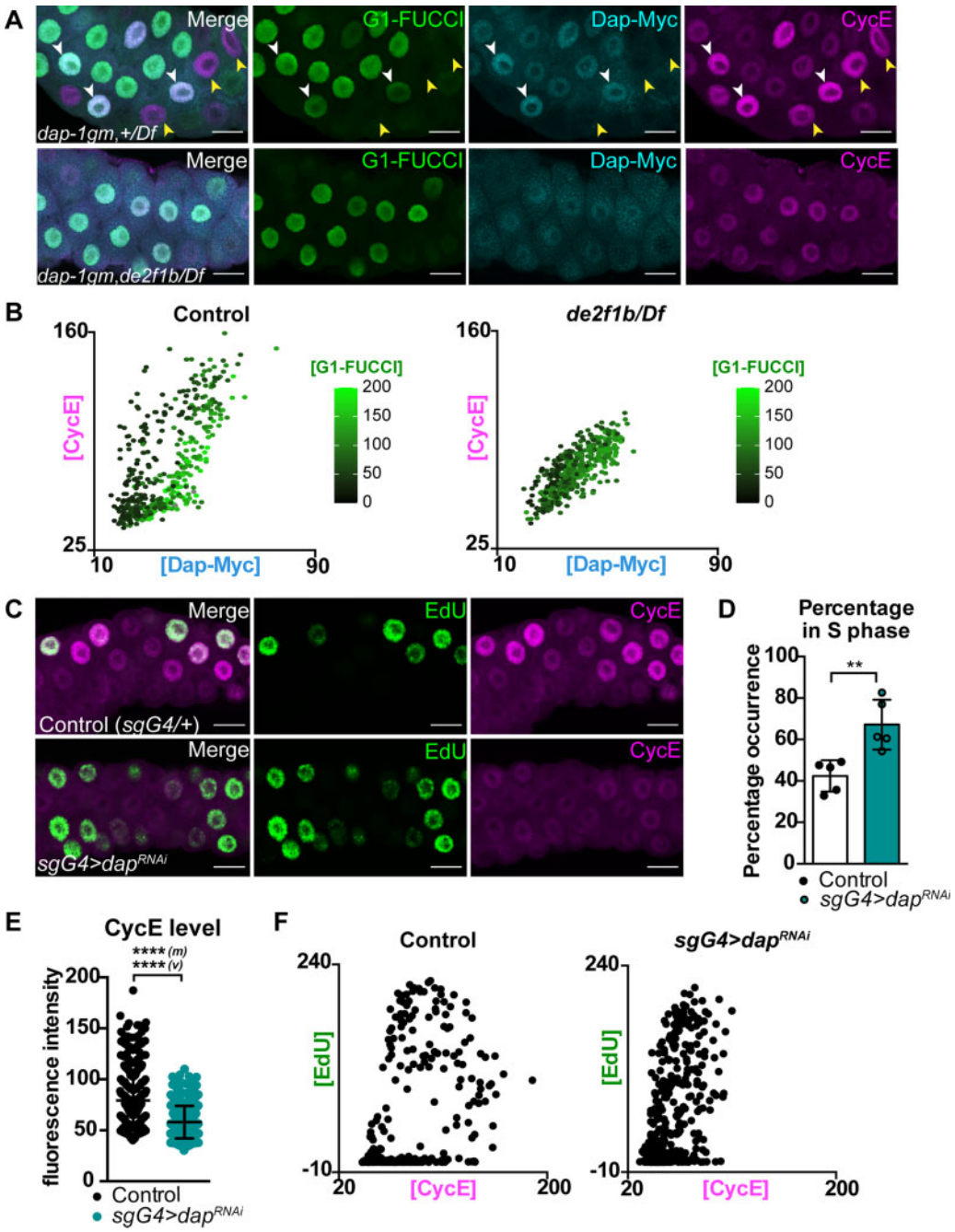

Figure 6 Dap limits the CycE–CDK2 activity in *de2f1b* salivary glands (A) Confocal micrographs of 80–85 h AEL salivary glands expressing Myc-tagged Dap construct (Dap-Myc) (cyan) and G1-FUCCI (green) labeled with CycE (magenta). White arrowheads indicate cells high in Dap-Myc, G1-FUCCI, and CycE. Yellow arrowheads indicate cells absent of Dap-Myc and G1-FUCCI with high CycE. (B) 2D scatter plots depicting expression levels of CycE (magenta) and Dap-Myc (cyan) relative to the G1-FUCCI expression per cell, which is represented by a gradation of black (low) to green (high) ($n = 5$/genotype). (C–F) The effect of depleting *dap* (*sgG4>dap*^{RNAi}) was determined. (C) Confocal micrographs of 80–85-h AEL salivary glands labeled with EdU (green) and CycE (Magenta). (D) The percentage of EdU-positive cells per salivary gland. Values represent the mean of five independent salivary glands and error bars indicate SD. $^{**}P \leq 0.01$. (E) A scatter plot showing CycE protein intensity from individual nuclei where mean (m) and variance showed a significant difference (v). $^{****}P \leq 0.0001$. (F) 2D scatter plots showing the relative expression pattern of EdU (green) and CycE (magenta) ($n = 5$/genotype). All scale bars = 25 μm.

suppressed the cell-cycle defect as shown in Figure 5D, separating G1-FUCCI and EdU-positive populations (Figure 5G). Moreover, *cycE* knockdown partially restored the nuclear DUP levels in *de2f1b* salivary glands (Supplementary Figure S2, C and D). Overall, these results show that the *de2f1b* mutation disrupts cell-cycle-dependent expression of CycE and leads to hyperactivation of CycE–Cdk2 during the endocycle.

Dap limits the CycE–Cdk2 activity in G phase

In both the ovary and the salivary glands, *dap* levels were reduced, whereas *cycE* levels were relatively unchanged (Figure 2A and Supplementary Figure S2A). To determine if Dap normally limits CycE–Cdk2 activity in the salivary gland and contributes to the endocycle defect in the *de2f1b* mutant, we determined the expression pattern of CycE, Dap, and G1-FUCCI. To visualize Dap

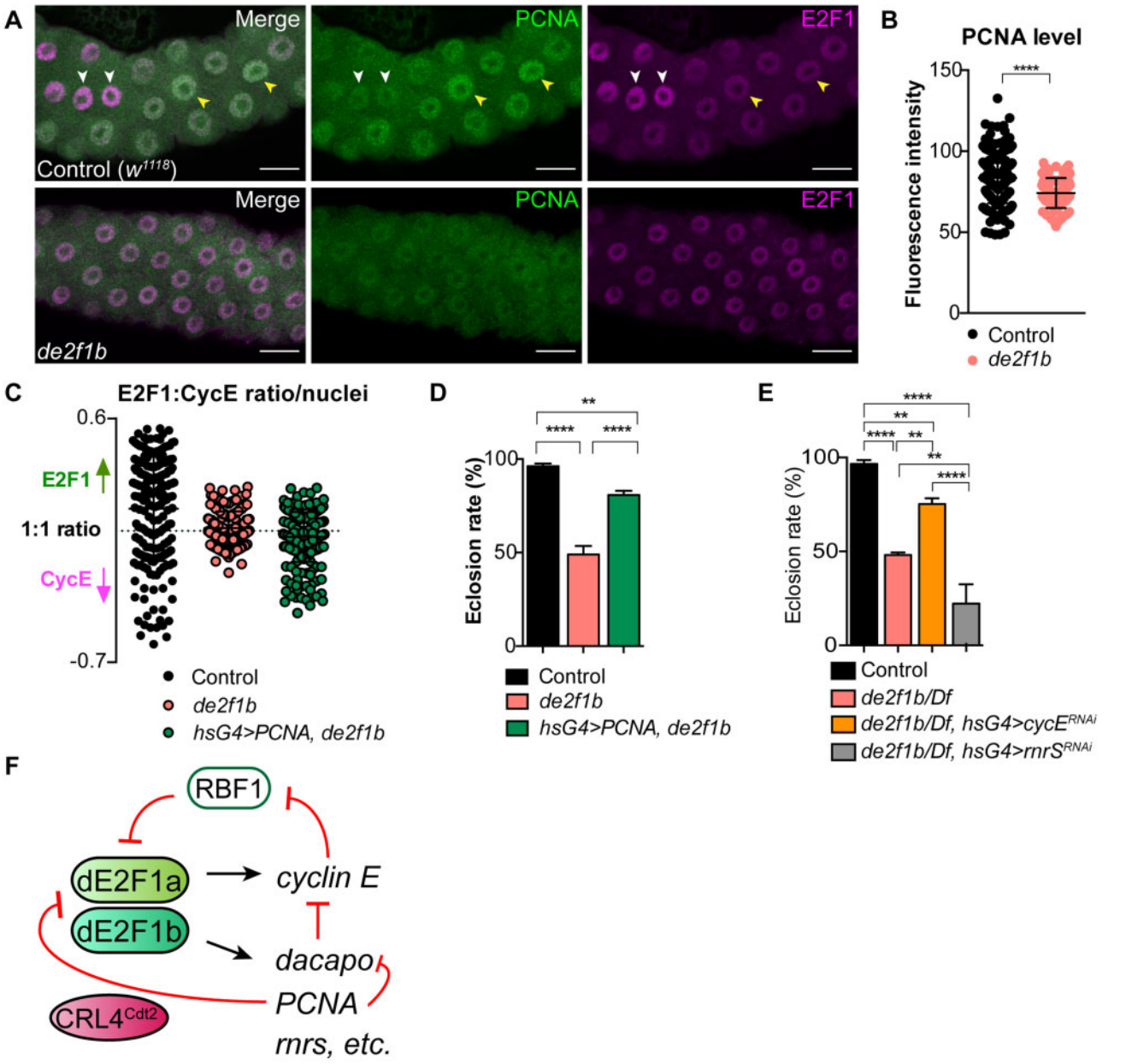

Figure 7 dE2F1b-dependent transcription of PCNA controls PIP box-mediated degradation and establishes a negative feedback loop. (A) Confocal micrographs of 80–85 h AEL Control and *de2f1b* salivary glands marked with PCNA (green) and dE2F1 (magenta). Yellow arrowheads indicate high dE2F1 and low PCNA cells. White arrowheads indicate low E2F1 and high PCNA cells. Scale bars = 25 μm. (B) A scatter plot comparing the differential nuclear levels of PCNA in control and *de2f1b* salivary glands. $^{****}P \leq 0.0001$. (C) dE2F1: CycE ratio plot for the indicated genotypes showing the partial restoration of high CycE cells upon PCNA expression in *de2f1b* salivary glands ($n = 5$/genotype). (D) Eclosion rate in the described genotypes where PCNA expression significantly rescued the eclosion defect of *de2f1b* flies. Error bars indicate SD from three independent experiments. $^{**}P \leq 0.01$; $^{****}P \leq 0.0001$. (E) Eclosion rates in control, *de2f1b/Df*, and *de2f1b/Df* expressing RNAi constructs against *cycE or rnrS* were compared. Error bars indicate SD from three independent experiments. $^{**}P \leq 0.01$; $^{****}P \leq 0.0001$. (F) A model illustrating the genetic circuitry controlled by dE2F1b where *dap* and *PCNA* are two crucial targets that control S-phase entry and exit, respectively.

protein, a Dap protein reporter (*dap-1gm*) was used. *dap-1gm* is a transgene containing a 6-kb 5′ regulatory region of Dap with the coding sequence tagged with 6XMyc epitopes on the C-terminus (Meyer *et al.* 2002). The analysis of CycE expression relative to G1-FUCCI and Dap (Dap-Myc) in control salivary glands (Figure 6A) revealed that cells expressing both CycE and Dap are often in G phase (white arrowheads in Figure 6A, upper panel). In contrast, CycE high and Dap low cells are in S phase (yellow arrowheads in Figure 6A, upper panel). The relationship between CycE and Dap relative to the cell cycle was best visualized in a scatter plot where the color gradation of each point from black (low) to green (high) represents the expression of G1-FUCCI (Figure 6B). In control salivary glands, higher G1-FUCCI expression was mainly associated with high Dap cells, indicating that Dap limits CycE–Cdk2 activity in the G phase. However, in *de2f1b* salivary glands, high Dap cells were lacking (Figure 6, A and B) and G- and S-phase cells could not be separated based on CycE and Dap levels (Figure 6B).

Although continuous expression of Dap can limit the endocycle (Swanson *et al.* 2015), a previous study suggested that Dap does not contribute to the periodic silencing of CycE–Cdk2 in the salivary gland (Zielke *et al.* 2011). This was largely based on the

lack of ploidy and size defects toward the end of the endocycle in Dap-deficient salivary glands. However, a detailed analysis of early L3 salivary glands that are actively undergoing the endocycle has not been performed to date. Therefore, we analyzed early and late L3 salivary glands that were subject to *dap* depletion and determined its effect on the cell cycle and the expression of CycE. Consistent with the previous findings, depletion of *dap* did not affect the overall ploidy in late L3 salivary glands (Supplementary Figure S3B). However, in early L3 salivary glands, a significant increase in the S-phase population was observed (Figure 6, C and D). In addition, CycE levels were significantly decreased in *dap*-depleted salivary glands (Figure 6, C and E). These results indicate that lowering the levels of *dap* expression of is sufficient for cells to enter S phase with lower levels of CycE. It also suggests that the decreased expression of Dap in *de2f1b* salivary glands (Figure 6A) likely contributes to the increase in S-phase population and the loss of CycE high cells (Figure 3, C and D). Unfortunately, we were unable to determine if restoring expression Dap in *de2f1b* salivary glands suppresses endocycle defects. Unlike in the ovary, the expression of Dap using the basal promoter activity of *hs-Gal4* strongly interfered with development, resulting in drastically smaller salivary glands (Supplementary Figure S3B).

dE2F1b-Dependent transcription of PCNA controls PIP box-mediated degradation and establishes a negative feedback loop

As described above, the destruction of dE2F1 in S phase requires chromatin-bound PCNA-dependent action of $CRL4^{Cdt2}$. The importance of PCNA in dE2F1 destruction can be easily visualized by depleting *PCNA* in the salivary gland. PCNA depletion disrupts the biphasic oscillation of dE2F1 and CycE (Supplementary Figure S3C). Corresponding to the transcript level (Figure 2A and Supplementary Figure S2A), nuclear PCNA levels were also significantly decreased in *de2f1b* salivary glands (Figure 7, A and B). In control salivary glands, cells with high PCNA levels have low dE2F1 expression (Figure 7A, yellow arrowhead) and low PCNA levels have high dE2F1 expression (Figure 7A, white arrowhead). In *de2f1b* salivary glands, cells with high PCNA levels were absent. To test if PCNA is a key component in *de2f1b* salivary glands for establishing the biphasic expression of CycE and dE2F1, PCNA was ectopically expressed using the basal promoter activity of *hs-Gal4*. Strikingly, expressing PCNA was sufficient to partially restore the biphasic oscillation of dE2F1 and CycE (Supplementary Figure S3D, asterisk region and Figure 7C). Unlike control cells, where a wide range of dE2F1 and CycE expressing nuclei were observed, *de2f1b* cells mostly have proportional levels of dE2F1 and CycE (Figure 7C). The expression of PCNA in *de2f1b* cells widened the range of CycE-expressing cells, indicating that the expression of PCNA partially restores biphasic expression of CycE and dE2F1. Importantly, analysis of late L3 salivary glands revealed that the ectopic expression of PCNA also improved the final ploidy of *de2f1b* salivary glands (Supplementary Figure S3E). Notably, we still observed the variable nuclear size defect seen in *de2f1b* salivary glands, suggesting that the nuclear size is independently regulated from ploidy control (Supplementary Figure S3F). In addition to the ploidy defect, ectopic PCNA expression significantly rescued the previously reported semi-lethality of *de2f1b* flies (Kim *et al.* 2018) (Figure 7D). The semi-lethality of *de2f1b* flies was also rescued by *cycE* depletion (Figure 7E). Our data collectively provide strong evidence that PCNA- and CycE-dependent processes are deregulated in *de2f1b* mutants.

Discussion

Previous genetic studies have established E2F as an important regulator of the endocycle (Edgar *et al.* 2014). In this study, we demonstrate that a critical function of dE2F1 during the endocycle is to limit CycE–Cdk2 activity. This was not mediated by transcriptional regulation of *cycE*, but rather by dE2F1b-dependent expression of the Cdk inhibitor, Dap. In addition, we showed that dE2F1b is the dE2F1 isoform that directly links E2F activity to its degradation in S phase via PCNA. Overall, we uncovered a previously unappreciated role of dE2F1 during the endocycle.

Analysis of *dDP* mutants and a hypomorphic allele of *de2f1*, $de2f1^{i2}$, demonstrated that dE2F1 activity is important for NC development (Myster *et al.* 2000; Royzman *et al.* 2002). However, neither *dDP* nor $de2f1^{i2}$ NCs showed a decrease in the expression of *cycE*, similar to what we observed in *de2f1b* NCs (Figure 2A). This is somewhat unexpected, given that *cycE* is considered a crucial downstream target of E2F. Although dE2F1a may maintain *cycE* expression in *de2f1b* ovaries, other factors may also contribute to *cycE* expression. Indeed, a transcription factor Apontic has been shown to regulate *cycE* during Drosophila eye development (Liu *et al.* 2014). However, for other G1/S genes, dE2F1b is responsible for maintaining their expression (Figure 2A and Supplementary Figure S2A) although E2F activity is generally dampened in endocycling tissues (Maqbool *et al.* 2010). Notably, the expression of G2/M genes was not affected by the *de2f1b* mutation, in line with a previous study, showing that the expression of G2/M genes is controlled by the MyB–MuvB (MMB) complex (Rotelli *et al.* 2019). It will be interesting to determine the effect of coactivating both the dE2F1b and the MMB complex. Perhaps, such manipulation can strongly drive mitotic cycles in normally endocycling tissues such as the salivary gland.

Studies in Drosophila adult rectal papillae have provided important mechanistic insights into the chromosome dispersal in polyploid cells. In this context, octopolyploid precursor cells disperse their polytene chromosomes before undergoing mitosis to give rise to rectal papillae (Fox *et al.* 2010). This dispersal process is regulated by Cohesin opening and not by Cohesin cleavage (Stormo and Fox 2016, 2019). Interestingly, NCs undergo a mitosis-like phase during NC chromosome dispersal (Dej and Spradling 1999) and Cohesin opening may be required for NCs as well. Given that limiting CycE–Cdk2 activity is required for chromosome dispersal in NCs (Lilly and Spradling 1996; Hong *et al.* 2007), it will be interesting to determine if the Cohesin-opening process is regulated by CycE–Cdk2 activity. In addition to limiting CycE–Cdk2 activity, alternative splicing seems to play an important function in chromosome dispersal. Mutations in genes involved in RNA splicing have been shown to interfere with the NC chromosome dispersal (Supplementary Table S5). Perhaps, these genes permit the proper expression of dE2F1b, an alternatively spliced form of *de2f1* (Kim *et al.* 2018).

de2f1b NCs show an abnormal pattern of heterochromatic markers (Figure 1D), which may arise from abnormal DNA replication in the heterochromatic region. A closer examination of EdU incorporation pattern revealed that a significant fraction of S-phase cells in *de2f1b* NCs (stages 3–5) contains EdU foci that overlap with DAPI dense regions (13 out of 127 EdU-positive cells, Supplementary Figure S3G). Nuclei with such EdU foci were very rare in control NCs (1 out of 97). Although this could be an indication of abnormal replication in the heterochromatin region, the possibility that it is a secondary consequence of the *de2f1b* remains. Since NCs fully replicate their genome from stage 3 to 5

(Dej and Spradling 1999), changes in E2F1 target gene expression (Figure 2A) may simply alter S-phase kinetics, making cells spend more time in the late S phase when the heterochromatin replicates. Nevertheless, proper control of CycE–Cdk2 activity seems to be vital for the maintenance of the heterochromatic region during the endocycle. Failure to properly downregulate CycE–Cdk2 activity either in S phase (Lilly and Spradling 1996; Hong *et al.* 2007) or in G phase (Figure 6, A and B) is sufficient to affect replication/organization of the heterochromatin.

Our data suggest that Dap is an integral part of the E2F-dependent regulation of the endocycle (Figure 6). A previous study showed that the expression of *dap* is normal in *de2f1* and *dDP* mutant embryos (de Nooij *et al.* 2000). We also observed that the expression of *dap* is largely unaffected in *de2f1b* eye disks (Supplementary Figure S3H). A possible way that dE2F1b affects the expression of Dap is through regulating the expression of CycE. It has been demonstrated that ectopic CycE expression is sufficient to promote the expression of Dap (de Nooij *et al.* 2000). However, this is less likely since the *cycE* RNA and protein levels are relatively unchanged in *de2f1b* salivary glands (Supplementary Figure S2, A and B; Figure 4D). Importantly, dE2F1 was shown to bind to the *dap* promoter during larval development (Korenjak *et al.* 2012), suggesting that *dap* is a direct target of dE2F1 although the effect on transcription may be tissue specific.

When Dap level is reduced, cells with high CycE levels are lacking in the salivary gland (Figures 4D and 6E). There are two possible mechanisms: first, Figure 6B suggests that in the absence of Dap, CycE–Cdk2 is hyperactive in G phase. This could allow cells to enter S phase without accumulating high levels of CycE and shorten the duration of G phase. Indeed, *de2f1b* mutant and Dap-depleted salivary glands have a larger fraction of cells in S phase (Figures 4D and 6E). However, the possibility of an extended S phase owing to higher CycE–Cdk2 activity cannot be excluded, as previously shown in the ovary (Lilly and Spradling 1996; Hong *et al.* 2007). Second, the protein stabilities of Dap and CycE may depend on one another. Previous studies demonstrated that ectopic expression of CycE is sufficient to increase the expression of Dap and that Dap-carrying mutations in the PIP degron stabilize CycE without affecting the mRNA level (de Nooij *et al.* 2000; Stadler *et al.* 2019). The latter study proposed that Dap's ability to inhibit CycE phosphorylation by Cdk2 reduces CycE ubiquitination via $SCF^{Fbxw7/Ago}$ (Stadler *et al.* 2019). Although the exact mechanism remains to be determined, Dap is undoubtedly an important factor in fine-tuning the CycE–Cdk2 activity during the endocycle.

Dap depletion itself does not result in ploidy defects in the salivary gland (Supplementary Figure S3B) (Zielke *et al.* 2011). This may be explained by the feed–forward relationship between CycE–Cdk2 and RBF1/dE2F1 (Figure 7F). Increased CycE–Cdk2 activity by *dap* depletion likely inactivates RBF1 more efficiently. This will hyperactivate dE2F1 and lead to a rapid accumulation of targets such as RNRs, MCMs, and DNA polymerases. Therefore, even if *dap*-deficient cells enter S phase earlier, this process ensures the expression of sufficient factors for S phase. The endocycle defect in *de2f1b* salivary glands disrupts this feed–forward relationship. In the absence of dE2F1b, S-phase genes cannot proportionally accumulate despite the increased CycE–Cdk2 activity (Figure 7F). This could slow down S-phase progression and may explain the reason why *de2f1b* salivary glands have lower ploidy (Kim *et al.* 2018).

Conclusion

Significantly, one of the important dE2F1b targets is PCNA. Failure to timely express PCNA results in the lack of the negative feedback regulation of dE2F1 and Dap in the S phase (Figure 7F) (Swanson *et al.* 2015; Stadler *et al.* 2019). As a consequence, dE2F1 becomes stabilized in the S phase and CycE is poorly downregulated, disrupting the biphasic expression of dE2F1 and CycE (Figure 4A). dE2F1, Dap, and DUP all contain PIP boxes and share redundant degradation mechanisms by $CRL4^{Cdt2}$ (Shibutani *et al.* 2008; Lee *et al.* 2010; Swanson *et al.* 2015). It has been previously proposed that $CRL4^{Cdt2}$ directs a sequential degradation of different proteins during G1/S phase (Coleman *et al.* 2015). It is probable that the sequence specificity of PIP-degrons in dE2F1, Dap, and DUP directs the timing of their degradation during the endocycle. Elucidating the molecular mechanism of the $CRL4^{Cdt2}$-mediated proteolysis will be crucial for further understanding of the regulatory network that controls endocycle progression.

Acknowledgments

The authors are grateful to T. Orr-Weaver (Whitehead Institute, MIT) and J. Nordman (Vanderbilt University) for sharing the anti-DUP antibody. The authors thank C. Lehner (University of Zurich) for sharing the *dap-1gm* fly stock. The authors also thank the Bloomington Stock Center, Drosophila Genetic Resource Center, and Vienna Drosophila Research Center for providing fly stocks. They also thank CIAN/ABIF for their assistance in confocal image acquisition.

M.K. and N.-S.M. conceptualized and designed experiments for this study. M.K. and K.D.S. conducted the investigation, data curation, and analysis. M.K. and N.-S.M. co-wrote this manuscript.

Funding

This study was supported by Natural Science and Engineering Research Council of Canada (RGPIN-2019-05699) and Canadian Institute of Health Research (162337).

Conflicts of interest

None declared.

Literature cited

Arias EE, Walter JC. 2006. PCNA functions as a molecular platform to trigger Cdt1 destruction and prevent re-replication. Nat Cell Biol. 8:84–90.

Calvi BR, Lilly MA, Spradling AC. 1998. Cell cycle control of chorion gene amplification. Genes Dev. 12:734–744.

Chen H-Z, Ouseph MM, Li J, Pécot T, Chokshi V *et al.* 2012. Canonical and atypical E2Fs regulate the mammalian endocycle. Nat Cell Biol. 14:1192–1202.

Coleman KE, Grant GD, Haggerty RA, Brantley K, Shibata E *et al.* 2015. Sequential replication-coupled destruction at G1/S ensures genome stability. Genes Dev. 29:1734–1746.

de Nooij JC, Graber KH, Hariharan IK. 2000. Expression of the cyclin-dependent kinase inhibitor Dacapo is regulated by Cyclin E. Mech Dev. 97:73–83.

de Nooij JC, Letendre MA, Hariharan IK. 1996. A cyclin-dependent kinase inhibitor, Dacapo, is necessary for timely exit from the cell cycle during Drosophila embryogenesis. Cell. 87:1237–1247.

Dej KJ, Spradling AC. 1999. The endocycle controls nurse cell polytene chromosome structure during Drosophila oogenesis. Development. 126:293–303.

Dimova DK, Dyson NJ. 2005. The E2F transcriptional network: old acquaintances with new faces. Oncogene. 24:2810–2826.

Du W. 2000. Suppression of the rbf null mutants by a de2f1 allele that lacks transactivation domain. Development. 127:367–379.

Edgar BA, Zielke N, Gutierrez C. 2014. Endocycles: a recurrent evolutionary innovation for post-mitotic cell growth. Nat Rev Mol Cell Biol. 15:197–210.

Fox DT, Gall JG, Spradling AC. 2010. Error-prone polyploid mitosis during normal Drosophila development. Genes Dev. 24: 2294–2302.

Hammond MP, Laird CD. 1985. Chromosome structure and DNA replication in nurse and follicle cells of *Drosophila melanogaster*. Chromosoma. 91:267–278.

Hong A, Narbonne-Reveau K, Riesgo-Escovar J, Fu H, Aladjem MI *et al.* 2007. The cyclin-dependent kinase inhibitor Dacapo promotes replication licensing during Drosophila endocycles. EMBO J. 26: 2071–2082.

Hsieh T-C, Nicolay BN, Frolov MV, Moon NS. 2010. Tuberous sclerosis complex 1 regulates dE2F1 expression during development and cooperates with RBF1 to control proliferation and survival. PLoS Genet. 6:e1001071.

Hu Y, Sopko R, Foos M, Kelley C, Flockhart I *et al.* 2013. FlyPrimerBank: an online database for *Drosophila melanogaster* gene expression analysis and knockdown evaluation of RNAi reagents. G3. 3:1607–1616.

Jin J, Arias EE, Chen J, Harper JW, Walter JC. 2006. A family of diverse Cul4-Ddb1-interacting proteins includes Cdt2, which is required for s phase destruction of the replication factor Cdt1. Mol Cell. 23: 709–721.

Kent LN, Leone G. 2019. The broken cycle: E2F dysfunction in cancer. Nat Rev Cancer. 19:1–338.

Keyes LN, Spradling AC. 1997. The Drosophila gene fs(2)cup interacts with otu to define a cytoplasmic pathway required for the structure and function of germ-line chromosomes. Development. 124: 1419–1431.

Kim M, Tang JP, Moon NS. 2018. An alternatively spliced form affecting the Marked Box domain of Drosophila E2F1 is required for proper cell cycle regulation. PLoS Genet. 14:e1007204.

Korenjak M, Anderssen E, Ramaswamy S, Whetstine JR, Dyson NJ. 2012. RBF binding to both canonical E2F targets and noncanonical targets depends on functional dE2F/dDP complexes. Mol Cell Biol. 32:4375–4387.

Lee HO, Zacharek SJ, Xiong Y, Duronio RJ. 2010. Cell type-dependent requirement for PIP box-regulated Cdt1 destruction during S phase. Mol Biol Cell. 21:3639–3653.

Li J, Ran C, Li E, Gordon F, Comstock G *et al.* 2008. Synergistic function of E2F7 and E2F8 is essential for cell survival and embryonic development. Dev Cell. 14:62–75.

Lilly MA, Duronio RJ. 2005. New insights into cell cycle control from the Drosophila endocycle. Oncogene. 24:2765–2775.

Lilly MA, Spradling AC. 1996. The Drosophila endocycle is controlled by Cyclin E and lacks a checkpoint ensuring S-phase completion. Genes Dev. 10:2514–2526.

Liu Q-X, Wang X-F, Ikeo K, Hirose S, Gehring WJ *et al.* 2014. Evolutionarily conserved transcription factor Apontic controls the G1/S progression by inducing cyclin E during eye development. Proc Natl Acad Sci USA. 111:9497–9502.

Maqbool SB, Mehrotra S, Kolpakas A, Durden C, Zhang B *et al.* 2010. Dampened activity of E2F1-DP and Myb-MuvB transcription factors in Drosophila endocycling cells. J Cell Sci. 123:4095–4106.

McGuire SE, Roman G, Davis RL. 2004. Gene expression systems in Drosophila: a synthesis of time and space. Trends Genet. 20: 384–391.

Meyer CA, Kramer I, Dittrich R, Marzodko S, Emmerich J *et al.* 2002. Drosophila p27Dacapo expression during embryogenesis is controlled by a complex regulatory region independent of cell cycle progression. Development. 129:319–328.

Moon NS, Dyson N. 2008. E2F7 and E2F8 keep the E2F family in balance. Dev Cell. 14:1–3.

Myster DL, Bonnette PC, Duronio RJ. 2000. A role for the DP subunit of the E2F transcription factor in axis determination during Drosophila oogenesis. Development. 127:3249–3261.

Narbonne-Reveau K, Senger S, Pal M, Herr A, Richardson HE *et al.* 2008. APC/CFzr/Cdh1 promotes cell cycle progression during the Drosophila endocycle. Development. 135:1451–1461.

Nordman J, Li S, Eng T, Macalpine D, Orr-Weaver TL. 2011. Developmental control of the DNA replication and transcription programs. Genome Res. 21:175–181.

Orr-Weaver TL. 2015. When bigger is better: the role of polyploidy in organogenesis. Trends Genet. 31:307–315.

Pandit SK, Westendorp B, Nantasanti S, Van Liere E, Tooten PCJ *et al.* 2012. E2F8 is essential for polyploidization in mammalian cells. Nat Cell Biol. 14:1181–1191.

Rotelli MD, Policastro RA, Bolling AM, Killion AW, Weinberg AJ *et al.* 2019. A Cyclin A—Myb-MuvB—Aurora B network regulates the choice between mitotic cycles and polyploid endoreplication cycles. PLoS Genet. 15:e1008253.

Royzman I, Austin RJ, Bosco G, Bell SP, Orr-Weaver TL. 1999. ORC localization in Drosophila follicle cells and the effects of mutations in dE2F and dDP. Genes Dev. 13:827–840.

Royzman I, Hayashi-Hagihara A, Dej KJ, Bosco G, Lee JY *et al.* 2002. The E2F cell cycle regulator is required for Drosophila nurse cell DNA replication and apoptosis. Mech. Dev. 119:225–237.

Rubin SM, Sage J, Skotheim JM. 2020. Integrating old and new paradigms of G1/S control. Mol Cell. 80:183–192.

Senga T, Sivaprasad U, Zhu W, Park JH, Arias EE *et al.* 2006. PCNA is a cofactor for Cdt1 degradation by CUL4/DDB1-mediated N-terminal ubiquitination. J Biol Chem. 281:6246–6252.

Sher N, Bell GW, Li S, Nordman J, Eng T *et al.* 2012. Developmental control of gene copy number by repression of replication initiation and fork progression. Genome Res. 22: 64–75.

Shibutani ST, la Cruz de AFA, Tran V, Turbyfill WJ, Reis T *et al.* 2008. Intrinsic negative cell cycle regulation provided by PIP box- and Cul4Cdt2-mediated destruction of E2f1 during S phase. Dev Cell. 15:890–900.

Stadler CB, Arefin B, Ekman H, Thor S. 2019. PIP degron-stabilized Dacapo/p21Cip1 and mutations in ago act in an anti-versus pro--proliferative manner, yet both trigger an increase in Cyclin E levels. Development. 146:dev175927.

Stormo BM, Fox DT. 2016. Distinct responses to reduplicated chromosomes require distinct Mad2 responses. Elife. 5: e15204.

Stormo BM, Fox DT. 2019. Interphase cohesin regulation ensures mitotic fidelity after genome reduplication. Mol Biol Cell. 30: 219–227.

Swanson CI, Meserve JH, McCarter PC, Thieme A, Mathew T *et al.* 2015. Expression of an S phase-stabilized version of the CDK inhibitor Dacapo can alter endoreplication. Development. 142: 4288–4298.

Thomer M, May NR, Aggarwal BD, Kwok G, Calvi BR. 2004. Drosophila double-parked is sufficient to induce re-replication

during development and is regulated by cyclin E/CDK2. Development. 131:4807–4818.

Volpe AM, Horowitz H, Grafer CM, Jackson SM, Berg CA. 2001. Drosophila rhino encodes a female-specific chromo-domain protein that affects chromosome structure and egg polarity. Genetics. 159:1117–1134.

Weng L, Zhu C, Xu J, Du W. 2003. Critical role of active repression by E2F and Rb proteins in endoreplication during Drosophila development. EMBO J. 22:3865–3875.

White AE, Leslie ME, Calvi BR, Marzluff WF, Duronio RJ. 2007. Developmental and cell cycle regulation of the Drosophila histone locus body. Mol Biol Cell. 18:2491–2502.

Whittaker AJ, Royzman I, Orr-Weaver TL. 2000. Drosophila double parked: a conserved, essential replication protein that colocalizes with the origin recognition complex and links DNA replication with mitosis and the down-regulation of S phase transcripts. Genes Dev. 14:1765–1776.

Yarosh W, Spradling AC. 2014. Incomplete replication generates somatic DNA alterations within Drosophila polytene salivary gland cells. Genes Dev. 28:1840–1855.

Zielke N, Kim KJ, Tran V, Shibutani ST, Bravo M-J *et al.* 2011. Control of Drosophila endocycles by E2F and CRL4(CDT2). Nature. 480: 123–127.

Zielke N, Korzelius J, van Straaten M, Bender K, Schuhknecht GFP *et al.* 2014. Fly-FUCCI: a versatile tool for studying cell proliferation in complex tissues. Cell Rep. 7:588–598.

Zielke N, Querings S, Rottig C, Lehner C, Sprenger F. 2008. The anaphase-promoting complex/cyclosome (APC/C) is required for rereplication control in endoreplication cycles. Genes Dev. 22: 1690–1703.

Communicating editor: R. Duronio